Stimulated Raman Scattering

DOI: 10.1002/anie.201400328

Live-Cell Stimulated Raman Scattering Imaging of Alkyne-Tagged Biomolecules**

Senlian Hong, Tao Chen, Yuntao Zhu, Ang Li, Yanyi Huang, and Xing Chen**

Abstract: *Alkynes can be metabolically incorporated into biomolecules including nucleic acids, proteins, lipids, and glycans. In addition to the clickable chemical reactivity, alkynes possess a unique Raman scattering within the Raman-silent region of a cell. Coupling this spectroscopic signature with Raman microscopy yields a new imaging modality beyond fluorescence and label-free microscopies. The bioorthogonal Raman imaging of various biomolecules tagged with an alkyne by a state-of-the-art Raman imaging technique, stimulated Raman scattering (SRS) microscopy, is reported. This imaging method affords non-invasiveness, high sensitivity, and molecular specificity and therefore should find broad applications in live-cell imaging.*

The alkyne has been used as a bioorthogonal chemical reporter that can be metabolically incorporated into various biomolecules including nucleic acids, proteins, glycans, and lipids.[1] In a subsequent step, the alkyne is chemically reacted with a fluorophore using the copper(I)-catalyzed azide–alkyne cycloaddition (CuAAC), that is, the click chemistry. This two-step chemical reporter strategy has emerged as a powerful tool for fluorescence imaging of biomolecules in live cells. Besides the clickable chemical reactivity, the alkyne intrinsically possesses a unique vibrational spectroscopic signature; the C≡C stretching vibration results in a Raman signal falling into the Raman-silent region, approximately 1800 to 2800 cm^{-1}, of a cell (see Figure S1 in the Supporting Information). Since all natural cellular molecules do not produce Raman signals in the silent region, the alkyne is Raman-spectroscopically bioorthogonal, enabling specific and background-free detection. In this regard, the alkyne serves as a bioorthogonal Raman reporter and may be exploited for visualizing biomolecules using Raman microscopy.[2,3] Importantly, direct Raman imaging of the alkyne obviates the burden of the second-step conjugation of fluorophores by click chemistry. Moreover, the alkyne is much smaller in size than fluorophores, rendering less perturbation to the biological systems.

The major obstacle in realizing this potentially powerful imaging modality is the poor sensitivity because of the notoriously small cross-section of the spontaneous Raman scattering. Surface-enhanced Raman scattering (SERS) has proven to be an effective method to overcome this challenge.[3] SERS improves the sensitivity up to the single-molecule level, owing to the electromagnetic enhancement.[4] In addition, SERS microscopy can be easily implemented into the conventional confocal Raman microscopes. However, SERS relies on the use of metallic nanostructures, commonly gold or silver nanoparticles, as enhancing substrates,[5] which practically complicate the experimental procedures with the need of bringing nanoparticles in close proximity to the cells. Moreover, SERS imaging is usually limited to cell-surface molecules such as glycans, whereas intracellular biomolecules like nucleic acids are not amenable to SERS imaging.

Alternatively, the newly emerged coherent Raman scattering microscopies such as stimulated Raman scattering (SRS) microscopy offer enhanced sensitivity over the spontaneous Raman scattering.[6,7] The sensitivity enhancement of SRS is achieved by exploiting the coherent nature of signal generation and does not require enhancing substrates. Furthermore, the intensity of the SRS signal is proportional to the analyte concentration, enabling quantitative imaging.[8] In contrast, signal quantification is relatively challenging for SERS[9] as well as coherent anti-Stokes Raman scattering (CARS),[10,11] another popular coherent Raman scattering technique. These advantageous features of SRS microscopy prompted us to explore its use for bioorthogonal Raman imaging.

Originally developed as a label-free imaging technique, SRS microscopy has enabled imaging of biomolecules including lipids, proteins, and DNA in live cells and in vivo.[10,12–14] Label-free SRS detects vibrational signals from the intrinsic chemical bonds of biomolecules, and thus suffers from poor molecular specificity, because many chemical bonds are shared by different types of biomolecules. We envisioned that coupling SRS technology with the bioorthogonal Raman reporters such as the alkyne would enable live imaging of biomolecules with both high sensitivity and molecular specificity. Herein, we demonstrate SRS imaging of four major

[*] S. Hong,[+] Y. Zhu, Prof. X. Chen
Beijing National Laboratory for Molecular Sciences
Department of Chemical Biology
College of Chemistry and Molecular Engineering
Synthetic and Functional Biomolecules Center
Peking-Tsinghua Center for Life Sciences
Peking University, Beijing 100871 (China)
E-mail: xingchen@pku.edu.cn

T. Chen,[+] A. Li, Prof. Y. Huang
Biodynamic Optical Imaging Center (BIOPIC)
College of Engineering, Peking University
Beijing 100871 (China)
E-mail: yanyi@pku.edu.cn

[+] These authors contributed equally to this work.

[**] This work was supported by the National Basic Research Program of China (973 Program; grant numbers 2012CB917303 to X.C. and 2011CB809106 to Y.H.) and the National Natural Science Foundation of China (grant numbers 91313301 to X.C. and 91313302 to Y.H.).

Supporting information for this article is available on the WWW under http://dx.doi.org/10.1002/anie.201400328.

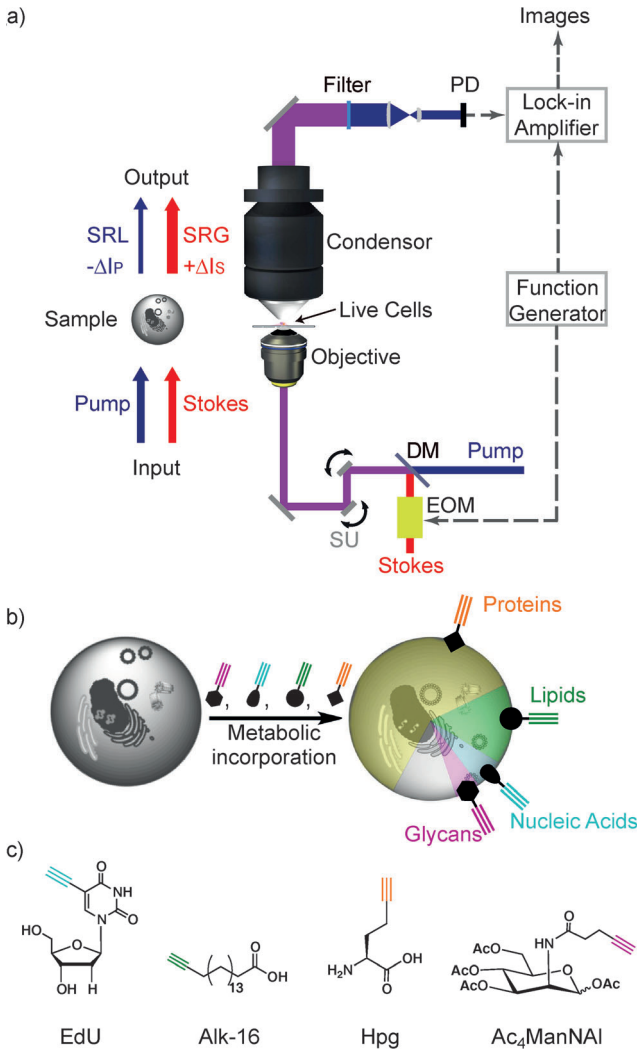

Figure 1. Live-cell SRS imaging of biomolecules metabolically labeled with an alkyne. a) Schematic illustration of the SRS process and the instrumental setup of SRS microscopy. When the pump and Stokes beams are co-linearly focused onto the sample, with a frequency difference matching the alkyne vibration, the pump beam experiences an energy loss $-\Delta I_p$ (Stimulated Raman Loss, SRL) while the Stokes beam an energy gain $+\Delta I_s$ (stimulated Raman gain, SRG). SU: scanning unit, PD: photodiode. b) Metabolic labeling of proteins, lipids, nucleic acids, and glycans by incubating the cells with the corresponding alkyne-bearing building blocks. The treated cells were then directly subjected to SRS microscopy. c) Chemical structures of 5-ethynyl-2′-deoxyuridine (EdU), 17-octadecynoic acid (Alk-16), homopropargylcine (Hpg), and peracetylated *N*-(4-pentynoyl)mannosamine (Ac_4ManNAl).

classes of biomolecules including nucleic acids, proteins, glycans, and lipids in live cells using the alkyne as the bioorthogonal Raman reporter (Figure 1).

Our in-house SRS microscope, schematically illustrated in Figure 1a, was built using a similar setup as previously reported.[15] To detect the vibrational frequency of the alkyne, we employed an integrated dual-wavelength picosecond pulsed laser with one beam (Stokes beam) fixed at 1064 nm, modulated at 10 MHz with an electrical optical modulator (EOM), and the other beam (pump beam) tuned to 868.2 nm through an integrated optical parametric oscillator (OPO). Two beams, with a frequency difference $\Delta\omega$ matching the vibrational frequency of the Raman reporter, were co-linearly introduced into a scanning microscope. A lock-in amplifier was used to extract the forward SRS signal (stimulated Raman loss, ΔI_p) from the background. The images were acquired by scanning the focal spot in two dimensions. Optical sectioning was applied for reconstruction of 3D SRS images.

Live-cell SRS microscopy was first demonstrated for label-free imaging of lipids using the C–H stretching of CH_2 groups at 2850 cm^{-1}.[10] This strategy collects signals from all lipids in a cell and has been used for studying fat storage.[16] Using spectrally tailored excitation[17] or hyperspectral SRS,[18] certain lipids with unique spectral features could be specifically imaged. However, it remains challenging to differentiate lipid types with similar chemical structures. For example, palmitic acid is an important type of fatty acid in eukaryotes and protein S-palmitosylation is essential for regulating the localization and function of many membrane-associated proteins.[19] Another major type of protein lipidation, *N*-myristoylation, is characterized by the addition of myristic acids.[20] These two saturated fatty acids structurally differ only in the chain length and therefore are essentially indistinguishable by the label-free SRS.

We therefore sought to specifically visualize the palmitic acids in live cells using SRS microscopy coupled with the alkyne tag. To do so, we employed ω-alkynyl palmitic acid (Alk-16), a palmitic acid analogue functionalized with an alkyne, as the bioorthogonal Raman reporter for palmitoylomes (Figure 1c).[21,22] The spontaneous Raman spectrum of Alk-16 showed a peak at 2120 cm^{-1} (Figure 2a). We mapped the SRS spectrum in a solution of Alk-16 (see Figure S2 in the Supporting Information) and on a live HeLa cell treated with Alk-16 (Figure 2a). The SRS spectra showed an alkyne peak at the same frequency of 2120 cm^{-1}, owing to the non-distorted nature of the SRS spectrum that is almost identical to the spontaneous Raman spectrum. We then acquired live-cell SRS images of palmitoylomes at 2120 cm^{-1}, which exhibited a strong signal of the alkyne (Figure 2b). The SRS microscopy of the alkyne revealed the distribution of the cellular Alk-16. When $\Delta\omega$ was tuned from the on-resonance of the alkyne (2120 cm^{-1}) to the off-resonance (2180 cm^{-1}), a minimal SRS signal was observed (Figure 2b and see Figure S3 in the Supporting Information). In addition, the control cells treated with natural palmitic acid exhibited minimal signal at 2120 cm^{-1}, confirming the molecular specificity of the SRS signal from the alkyne.

Two-color SRS imaging was performed by using 2120 cm^{-1} for the alkyne and 2850 cm^{-1} for CH_2 (Figure 2b and c). The SRS imaging at 2850 cm^{-1} presumably reflected the distribution of the total lipids in the cells, while the SRS imaging of the alkyne specifically exhibited the cellular location of palmitic acids. The SRS signal intensity of Alk-16 increased in a dose-dependent manner, highlighting the quantitative feature of SRS microscopy (Figure 2d). The palmitic acid distribution revealed by the SRS images are similar to the fluorescence images obtained on cell treated with Alk-16, followed by fixation, permeabilization, and click-labeling (see Figure S4 in the Supporting Information).[21]

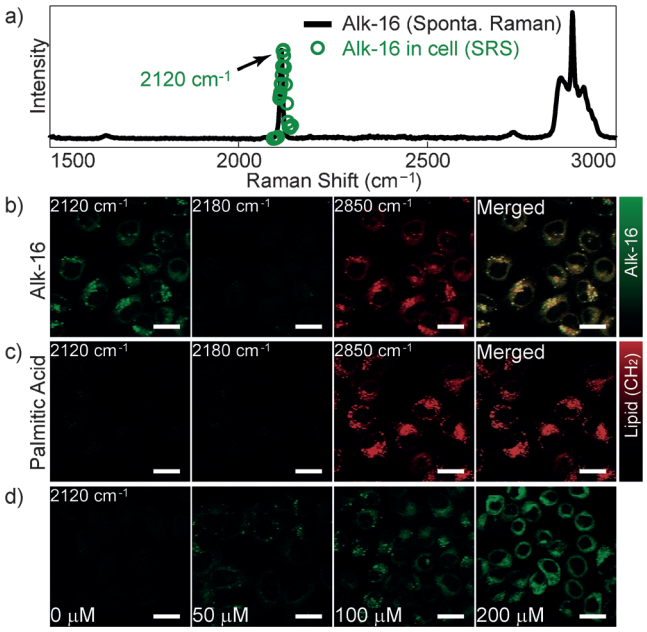

Figure 2. SRS imaging of Alk-16 in live cells. a) Spontaneous Raman spectrum of pure Alk-16 (black line), with respect to the SRS spectrum of Alk-16 in live cells (green circle). b) SRS images of HeLa cells treated with 100 μM Alk-16 for 16 h. Images shown from left to right are the alkyne on-resonance (2120 cm^{-1}), alkyne off-resonance (2180 cm^{-1}), total lipids (2850 cm^{-1}), and merged image of Alk-16 and total lipids. c) SRS images of HeLa cells fed with natural palmitic acids. d) SRS images of cells treated with Alk-16 at varied concentrations. All images (256×256 pixels) were obtained using a 40 μs pixel dwell time. Scale bars: 20 μm.

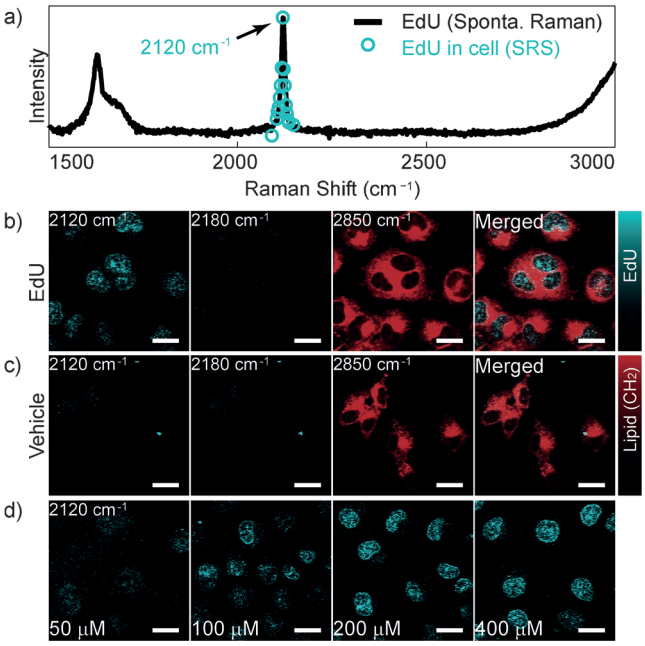

Figure 3. SRS imaging of EdU in live cells. a) Spontaneous Raman spectrum of pure EdU (black line), with respect to SRS spectrum of EdU in live cells (cyan circle). b) SRS images of HeLa cells treated with 200 μM EdU for 18 h. Images shown from left to right are the alkyne on-resonance (2120 cm^{-1}), alkyne off-resonance (2180 cm^{-1}), total lipids (2850 cm^{-1}) and merged images of EdU and total lipids. c) SRS images of HeLa cells cultured in the absence of EdU. d) SRS images of cells treated with EdU at varied concentrations. All images (256×256 pixels) were obtained using a 40 μs pixel dwell time. Scale bars: 20 μm.

Importantly, the SRS imaging of the alkyne not only affords a more convenient imaging procedure by virtue of requiring no additional click-labeling steps, but also enables live-cell imaging that is implausible by fluorescence microscopy in this case because of the need of fixation and permeabilization.

This methodology can be readily applied to visualize other types of lipids, given the availability of a variety of alkyne-containing lipid analogues.[23] As an additional showcase of SRS imaging of lipids using the alkyne reporter, we visualized the choline-containing phospholipids in live cells using the propargylcholine, an alkyne-functionalized choline analogue (see Figure S5 in the Supporting Information).[24] Notably, the alkyne peak of propargylcholine shifts to 2138 cm^{-1}, probably because of the neighboring chemical environment. In agreement with our observation, an array of alkyne-containing compounds with different neighboring functional groups were reported to exhibit varied alkyne frequencies.[25] This feature highlights the potential applications of multi-color SRS imaging of the alkyne for simultaneous visualization of multiple lipids with molecular specificity in live cells.

We next sought to extend the bioorthogonal SRS imaging to other classes of biomolecules. To image DNA, we employed 5-ethynyl-2′-deoxyuridine (EdU), an alkyne-bearing thymidine analogue, which is metabolically incorporated into replicating DNA by partly substituting thymidine.[26] The alkyne of EdU also processes a SRS peak at 2120 cm^{-1} (Figure 3a). SRS imaging of HeLa cells treated with EdU revealed intense alkyne signals in the nuclei (Figure 3b). The alkyne staining of nuclei exhibited a positive correlation between the SRS signal intensity and the concentration of EdU (Figure 3d). The incorporation of EdU was abolished by treatment with hydroxyurea (see Figure S6 in the Supporting Information), indicating that the SRS signal of the alkyne observed in the nuclei resulted from EdU incorporation during the DNA synthesis. It should be noted that despite its popular use, EdU exhibits toxicity and causes cell-cycle arrest over prolonged experimental periods.[27,28] As a potential alternative, another recently developed alkyne-containing thymidine, (2′*S*)-2′-deoxy-2′-fluoro-5-ethynyluridine (F-ara-EdU), which exhibited less toxicity, may be exploited for SRS imaging of DNA for experiments requiring long-term observation.[29]

The alkyne is not only chemically stable towards the reactive species in a cell, but also photostable, that is, the Raman signal intensity of the alkyne does not decay upon continuous monitoring for a prolonged time (see Figure S7 in the Supporting Information). The photostability of the alkyne in SRS makes it a valuable alternative for applications where photobleaching of fluorescence is problematic. Furthermore, we determined the SRS detection limit of EdU to be at the level of hundreds of μM, that is, tens of thousands of EdU molecules inside the focal volume, in our experimental setup (see Figure S8 in the Supporting Information). In addition, the SRS microscopy has the intrinsic optical sectioning capability, as demonstrated by the 3D imaging of EdU-

treated HeLa cells (see Figure S9 in the Supporting Information).

Compared with imaging EdU using the slit-scanning Raman microscopy,[2] SRS offers a much faster imaging speed. Each image (256 × 256 pixel) requires an acquisition time less than 1 s, which is over 1000-fold faster than the slit-scanning Raman microscopy. The fast imaging speed and the near-infrared excitation of SRS imaging renders minimal photodamage to the cells. Notably, the slit-scanning or conventional Raman microscopy records wide-range spectra for each pixel, while our SRS method uses narrow-band signals for image reconstruction.

Finally, we demonstrated the SRS imaging of proteins and glycans using the alkyne as the Raman reporter (Figure 4). To

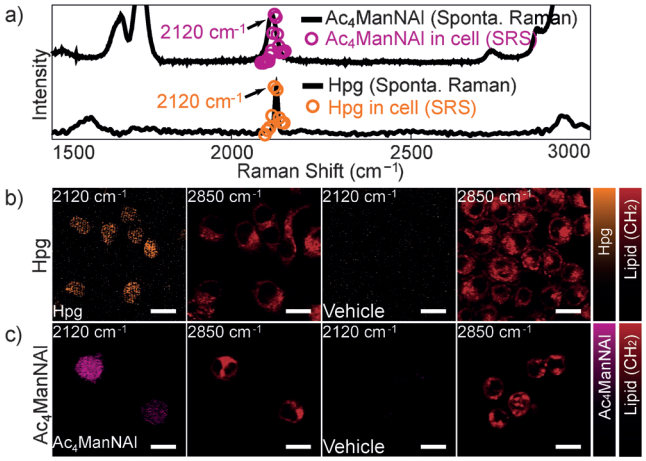

Figure 4. SRS imaging of Hpg and Ac_4ManNAl in live cells. a) Spontaneous Raman spectra of pure EdU and Ac_4ManNAl (black lines), with respect to SRS spectra of Hpg (orange circle) and Ac_4ManNAl (magenta circle) in live cells. b) SRS images of HeLa cells treated with 4 mM Hpg or with vehicle for 24 h. Images shown from left to right are the alkyne on-resonance (2120 cm^{-1}), total lipids (2850 cm^{-1}) of respect sample. c) SRS images of K20 cells treated with 400 μM Ac_4ManNAl or with vehicle for 72 h. Images shown from left to right are the alkyne on-resonance (2120 cm^{-1}), total lipids (2850 cm^{-1}) of respect sample. All images (256 × 256 pixels) were in using a 40 μs pixel dwell time. Scale bars: 20 μm.

image proteins, we treated HeLa cells with homopropargylglycine (Hpg), an alkyne-containing noncanonical amino acid serving as a surrogate for methionine.[30] SRS imaging at 2120 cm^{-1} showed the distribution of the newly-synthesized proteins that were metabolically labeled with Hpg (Figure 4b). The alkyne signal appears to condense in nucleolar structures, in agreement with the previous observation using click-labeling.[22] To demonstrate glycan visualization, we performed SRS imaging on K20 cells treated with peracetylated *N*-(4-*p*entynoyl)mannosamine (Ac_4ManNAl), which can be metabolically converted to the corresponding sialic acid (SiaNAl) and incorporated into the sialylated glycans. SRS imaging at 2120 cm^{-1} exhibited the cellular distribution of the alkyne, which probably included the free ManNAl, metabolic intermediates, and sialylated glycans (Figure 4c).

In summary, we have developed a bioorthogonal SRS imaging method for visualizing various biomolecules in live cells. The alkyne, which is small, non-perturbative, and possesses a Raman signal in the silent region, functioned as a bioorthognal Raman reporter. Lipids, nucleic acids, proteins, and glycans were metabolically labeled with the alkyne, which enables live-cell SRS imaging with molecular specificity. In addition to an alkyne, the carbon–deuterium (C–D) bond also processes a Raman resonance within the silent region and isotopic substitution with deuterium has been explored for cellular imaging of lipids, proteins, and small molecule drugs.[31–36] While the C–D bond requires only isotopic substitution and thus is more biocompatible, the alkyne offers a greater Raman cross-section.[25] Notably, there are some alkyne-bearing drugs that are in current clinical use and our SRS imaging method will be valuable for the pharmacological studies. Furthermore, many other functional groups fulfil the criteria of the bioorthogonal Raman reporters such as azide and nitrile,[3] and isotopic substitution with deuterium, carbon-13, or nitrogen-15 can further expand the "color palette". The bioorthogonal SRS imaging methodology complements the fluorescence and label-free microscopies by offering a new imaging modality that combines some advantageous features from both. With further improvements on the detection sensitivity, it will become achievable to specifically image the low abundant biomolecules in live cells with SRS microscopy.

Received: January 12, 2014
Revised: February 26, 2014
Published online: April 17, 2014

Keywords: biomolecules · bioorthogonality · Raman imaging · stimulated Raman scattering

[1] M. Grammel, H. C. Hang, *Nat. Chem. Biol.* **2013**, *9*, 475–484.
[2] H. Yamakoshi, K. Dodo, M. Okada, J. Ando, A. Palonpon, K. Fujita, S. Kawata, M. Sodeoka, *J. Am. Chem. Soc.* **2011**, *133*, 6102–6105.
[3] L. Lin, X. Tian, S. Hong, P. Dai, Q. You, R. Wang, L. Feng, C. Xie, Z. Q. Tian, X. Chen, *Angew. Chem.* **2013**, *125*, 7407–7412; *Angew. Chem. Int. Ed.* **2013**, *52*, 7266–7271.
[4] E. C. Le Ru, P. G. Etchegoin, *Annu. Rev. Phys. Chem.* **2012**, *63*, 65–87.
[5] P. L. Stiles, J. A. Dieringer, N. C. Shah, R. P. Van Duyne, *Annu. Rev. Anal. Chem.* **2008**, *1*, 601–626.
[6] E. Ploetz, S. Laimgruber, S. Berner, W. Zinth, P. Gilch, *Appl. Phys. B* **2007**, *87*, 389–393.
[7] W. Min, C. W. Freudiger, S. Lu, X. S. Xie, *Annu. Rev. Phys. Chem.* **2011**, *62*, 507–530.
[8] D. Fu, F.-K. Lu, X. Zhang, C. Freudiger, D. R. Pernik, G. Holtom, X. S. Xie, *J. Am. Chem. Soc.* **2012**, *134*, 3623–3626.
[9] K. Kneipp, H. Kneipp, I. Itzkan, R. R. Dasari, M. S. Feld, *J. Phys. Condens. Matter* **2002**, *14*, R597.
[10] C. W. Freudiger, W. Min, B. G. Saar, S. Lu, G. R. Holtom, C. He, J. C. Tsai, J. X. Kang, X. S. Xie, *Science* **2008**, *322*, 1857–1861.
[11] T. Weeks, I. Schie, L. J. den Hartigh, J. C. Rutledge, T. Huser, *J. Biomed. Opt.* **2011**, *16*, 021117.
[12] B. G. Saar, C. W. Freudiger, J. Reichman, C. M. Stanley, G. R. Holtom, X. S. Xie, *Science* **2010**, *330*, 1368–1370.

[13] M. Ji, D. A. Orringer, C. W. Freudiger, S. Ramkissoon, X. Liu, D. Lau, A. J. Golby, I. Norton, M. Hayashi, N. Y. R. Agar, et al., *Sci. Transl. Med.* **2013**, *5*, 201ra119.
[14] X. Zhang, M. B. J. Roeffaers, S. Basu, J. R. Daniele, D. Fu, C. W. Freudiger, G. R. Holtom, X. S. Xie, *ChemPhysChem* **2012**, *13*, 1054 – 1059.
[15] Z. Yu, T. Chen, X. Zhang, D. Fu, X. Liao, J. Shen, X. Liu, B. Zhang, X. S. Xie, X.-D. Su, et al., *Chem. Sci.* **2012**, *3*, 2646.
[16] M. C. Wang, W. Min, C. W. Freudiger, G. Ruvkun, X. S. Xie, *Nat. Methods* **2011**, *8*, 135 – 138.
[17] C. W. Freudiger, W. Min, G. R. Holtom, B. Xu, M. Dantus, X. Sunney Xie, *Nat. Photonics* **2011**, *5*, 103 – 109.
[18] P. Wang, J. Li, P. Wang, C.-R. Hu, D. Zhang, M. Sturek, J.-X. Cheng, *Angew. Chem.* **2013**, *125*, 13280 – 13284; *Angew. Chem. Int. Ed.* **2013**, *52*, 13042 – 13046.
[19] M. E. Linder, R. J. Deschenes, *Nat. Rev. Mol. Cell Biol.* **2007**, *8*, 74 – 84.
[20] M. D. Resh, *Nat. Chem. Biol.* **2006**, *2*, 584 – 590.
[21] G. Charron, M. M. Zhang, J. S. Yount, J. Wilson, A. S. Raghavan, E. Shamir, H. C. Hang, *J. Am. Chem. Soc.* **2009**, *131*, 4967 – 4975.
[22] J. S. Yount, B. Moltedo, Y.-Y. Yang, G. Charron, T. M. Moran, C. B. López, H. C. Hang, *Nat. Chem. Biol.* **2010**, *6*, 610 – 614.
[23] H. C. Hang, J. P. Wilson, G. Charron, *Acc. Chem. Res.* **2011**, *44*, 699 – 708.
[24] C. Y. Jao, M. Roth, R. Welti, A. Salic, *Proc. Natl. Acad. Sci. USA* **2009**, *106*, 15332 – 15337.
[25] H. Yamakoshi, K. Dodo, A. Palonpon, J. Ando, K. Fujita, S. Kawata, M. Sodeoka, *J. Am. Chem. Soc.* **2012**, *134*, 20681 – 20689.
[26] A. Salic, T. J. Mitchison, *Proc. Natl. Acad. Sci. USA* **2008**, *105*, 2415 – 2420.
[27] P. Cappella, F. Gasparri, M. Pulici, J. Moll, *Cytometry Part A* **2008**, *73*, 626 – 636.
[28] S. Diermeier-Daucher, S. T. Clarke, D. Hill, A. Vollmann-Zwerenz, J. A. Bradford, G. Brockhoff, *Cytometry Part A* **2009**, *75*, 535 – 546.
[29] A. B. Neef, N. W. Luedtke, *Proc. Natl. Acad. Sci. USA* **2011**, *108*, 20404 – 20409.
[30] K. E. Beatty, J. C. Liu, F. Xie, D. C. Dieterich, E. M. Schuman, Q. Wang, D. A. Tirrell, *Angew. Chem.* **2006**, *118*, 7524 – 7527; *Angew. Chem. Int. Ed.* **2006**, *45*, 7364 – 7367.
[31] J. P. Pezacki, J. A. Blake, D. C. Danielson, D. C. Kennedy, R. K. Lyn, R. Singaravelu, *Nat. Chem. Biol.* **2011**, *7*, 137 – 145.
[32] X. S. Xie, J. Yu, W. Y. Yang, *Science* **2006**, *312*, 228 – 230.
[33] M. Miljković, T. Chernenko, M. J. Romeo, B. Bird, C. Matthäus, M. Diem, *Analyst* **2010**, *135*, 2002 – 2013.
[34] C. Matthäus, C. Krafft, B. Dietzek, B. R. Brehm, S. Lorkowski, J. Popp, *Anal. Chem.* **2012**, *84*, 8549 – 8556.
[35] L. Wei, Y. Yu, Y. Shen, M. C. Wang, W. Min, *Proc. Natl. Acad. Sci. USA* **2013**, *110*, 11226 – 11231.
[36] G. Bergner, C. R. Albert, M. Schiller, G. Bringmann, T. Schirmeister, B. Dietzek, S. Niebling, S. Schlücker, J. Popp, *Analyst* **2011**, *136*, 3686 – 3693.

